Chinese Chemical Letters 31 (2020) 2287–2294

Contents lists available at ScienceDirect

Chinese Chemical Letters

journal homepage: www.elsevier.com/locate/cclet

Communication

Construction of SiO_2-TiO_2/g-C_3N_4 composite photocatalyst for hydrogen production and pollutant degradation: Insight into the effect of SiO_2

Sijia Sun[a], Hao Ding[a,*], Lefu Mei[a,*], Ying Chen[a], Qiang Hao[b], Wanting Chen[a], Zhuoqun Xu[a], Daimei Chen[a,*]

[a] Beijing Key Laboratory of Materials Utilization of Nonmetallic Minerals and Solid Wastes, National Laboratory of Mineral Materials, School of Materials Science and Technology, China University of Geosciences, Beijing 100083, China
[b] Centre for Technology in Water and Wastewater (CTWW), School of Civil and Environmental Engineering, University of Technology Sydney (UTS), Ultimo, NSW 2007, Australia

ARTICLE INFO

Article history:
Received 31 December 2019
Received in revised form 11 February 2020
Accepted 1 March 2020
Available online 9 March 2020

Keywords:
SiO_2 carrier
Heterostructure
Photocatalyst
g-C_3N_4
TiO_2

ABSTRACT

Using low-cost precipitated silica (SiO_2) as the carrier, a ternary SiO_2-TiO_2/g-C_3N_4 composite photocatalyst was prepared via the sol-gel method associated with a wet-grinding process. The as-prepared composite exhibits photocatalytic hydrogen production and pollutant degradation performance under solar-like irradiation. The effect of SiO_2 carrier on the properties of the heterostructure between TiO_2 and g-C_3N_4 (CN) was systematically studied. It is found that SiO_2 has important effects on promoting the interaction between TiO_2 and CN. The particle size of TiO_2 and CN was obviously reduced during the calcination process due to the effects of SiO_2. Especially, the TiO_2 particles exhibit monodispersed state with particle size below 10 nm (quantum dots), resulting in the improvement of the contact area and the interaction between TiO_2 and CN, and leading to the formation of efficient TiO_2/CN Z-scheme heterostructure in SiO_2-TiO_2/CN. Besides, the introduction of SiO_2 can increase the specific surface area and light absorption of SiO_2-TiO_2/CN, further promoting the photocatalytic reaction. As expected, the optimum SiO_2-TiO_2/CN composite exhibits 12.3, 3.1 and 2.9 times higher photocatalytic hydrogen production rate than that of SiO_2-TiO_2, CN and TiO_2/CN under solar-like irradiation, while the photocatalytic active component in SiO_2-TiO_2/CN is only about 60 wt%. Moreover, the rhodamine B degradation rate of SiO_2-TiO_2/CN is also higher than that of SiO_2-TiO_2, CN and TiO_2/CN.

The continuous consumption of non-renewable energy and increasing environmental pollution have caused a serious crisis for human development. Solar energy is considered as an ideal way to solve these problems because it is clean, green and has wide resource [1,2]. Photocatalytic hydrogen generation has become an attractive approach for solar energy conversion [3]. The g-C_3N_4 (CN) exhibits good performance for hydrogen production and pollutant degradation under visible-light irradiation because of its narrow bandgap and appropriate band structure. It has advantages of facile synthesis, low cost, non-toxicity and good stability [4–6]. However, there are several problems of CN which limits its application, including the low surface area and the short separation lifetime of photogenerated charge carriers [7–9]. Coupling CN with other semiconductor photocatalyst, such as TiO_2, ZnO and CdS, to constructive heterojunctions is an efficient way to accelerate the separation of electron-hole pairs [10–13]. Compared with the traditional type-II heterostructure, the Z-Scheme structure has attracted much attention because it can reduce the recombination efficiency of the electron-hole pairs, without reducing the reduction/oxidation potentials of electrons/holes [14]. Therefore, several CN-based Z-scheme photocatalysts have been developed to superior photocatalytic reduction and oxidation and activities, such as ZnO/CN, SnS_2/CN and WO_3/CN heterojunctions [15–17].

TiO_2 is one of the most widely studied photocatalysts because it is stable and nontoxic [18]. The band structure of TiO_2 can match with that of CN, determining that it can couple with CN to form heterostructure [19–21]. However, the construction of TiO_2/CN composite still needs to be improved in the following three

* Corresponding authors.
E-mail addresses: dinghao113@126.com (H. Ding), mlf@cugb.edu.cn (L. Mei), chendaimei@cugb.edu.cn (D. Chen).

https://doi.org/10.1016/j.cclet.2020.03.026

aspects: Firstly, the nano-TiO_2 and CN always agglomerate into aggregates with larger apparent particle size, which makes it difficult for TiO_2 and CN to combine uniformly with large contact area. Moreover, the prepared TiO_2/CN composite has low specific surface area and less reaction site, which limits the photocatalytic performance enhancement. Secondly, CN is an organic polymer semiconductor, which leads to its poor combination with transition metal semiconductor without strong external forces, resulting in weak interaction of heterostructures [22]. Thirdly, TiO_2 particles with large size tend to exhibit long-range ordered crystal arrangement, while CN exhibits weakly ordered degree. The difference in crystal structure between them will reduce the quality of the heterostructures. These problems will be adverse to the formation of efficient Z-scheme structure, and it may significantly affect the stability and photocatalytic activity of TiO_2/CN composites. Several attempts have been carried out to construct TiO_2/CN Z-scheme heterostructure, such as the doping of TiO_2, introducing a conductor (always noble metal) between TiO_2 and CN and adjusting the crystal plane and morphology of TiO_2 to couple with CN [23–26]. However, there are few studies about the construction of efficient TiO_2/CN Z-scheme heterostructure through introducing a carrier to change the particle size, crystallinity and interfacial bonding properties of TiO_2 and CN.

SiO_2 is often used as a photocatalyst carrier because it has abundant surface hydroxyl groups and can reduce the particle size of the loaded photocatalyst, which also can improve the dispersivity and stability of photocatalysts and increase the surface area [27,28]. More importantly, SiO_2 also has a large negative surface charge in water, which can affect the migration behavior of photogenerated electrons in TiO_2 and CN. Therefore, it is expected to enhance the performance of TiO_2/CN heterostructure and promoted the formation of Z-scheme heterostructure by introducing SiO_2 into the TiO_2/CN system to prepare ternary composite photocatalysts. However, SiO_2 nanoparticles are usually prepared by sol-gel method with complex process and high cost [29–31]. Moreover, the previous studies always focused on the preparation of SiO_2/semiconductor binary composite photocatalysts, such as SiO_2/TiO_2 or SiO_2/ZnO [32,33]. There is a lack of study on constructing a ternary composite photocatalyst by loading two kinds of semiconductors on SiO_2 to get better synergy. Therefore, it is of great significance for developing cheap SiO_2 raw materials and an efficient compound method to prepare the SiO_2-based ternary composite photocatalysts. Besides, the mechanism of SiO_2 for the enhanced photocatalytic performance is still not clear.

In this study, the SiO_2-TiO_2/CN ternary composite photocatalyst was prepared. Through the introduction of SiO_2, the particle size of TiO_2 and CN can be reduced, and the contact area and structural matching degree between TiO_2 and CN can be improved. The close bonding between highly dispersed TiO_2 and CN can form generous charge transport channels. Therefore, without the existence of the electron conductor, an efficient TiO_2/CN Z-scheme heterostructure is constructed. The morphology, structure and photocatalytic performance of the as-prepared SiO_2-TiO_2/CN composites were characterized. Especially, the effects of SiO_2 on the interaction between TiO_2 and CN and the performance improvement of SiO_2-TiO_2/CN were systematically discussed. The findings of this study have important implications for the development of novel, low-cost and efficient heterostructure photocatalytic materials.

The detailed information of the materials and reagents used in this study is listed as follows. The SiO_2 raw material was purchased from Henan Jiaozuo Fluoride New Energy Technology Co., Ltd. (Henan, China). Tetrabutyltitanate (TBOT) and chloroplatinic acid were bought from Aladdin Reagent Co., Ltd, and analytical pure ethanol and acetylacetone were purchased from Beijing Chemical Works and Xilong scientific Co., Ltd. The chemical purity melamine was provided by Sinpharm Chemical Reagent Co., Ltd. Deionized water was also used in the whole experiment.

The SiO_2-TiO_2 composite was prepared by sol-gel method, and the details are as follows. Firstly, 10 g of SiO_2 was dispersed in 120 mL of ethanol solution under continuous stirring. Next, 10 mL of TBOT and the mixture of acetylacetone and water (15 mL of acetylacetone and 120 mL of water) were added into the above SiO_2-ethanol slurry. The above mixture was stirred for 24 h at room temperature to ensure the uniform loading of $TiO_2 \cdot nH_2O$ on the SiO_2 surface. Next, the obtained product was placed in a drying oven and was kept at 80 °C for 12 h. Finally, the sample was calcined by a muffle furnace with the temperature of 600 °C for 2 h with the heating rate of 5 °C/min. The mass fraction of TiO_2 in SiO_2-TiO_2 is 9.88 wt% according to the XRF analysis. As shown in the preparation schematic diagram (Scheme 1), the preparation of SiO_2-TiO_2/CN composite was conducted according to the following steps: Firstly, 2 g of as-prepared SiO_2-TiO_2 powder was added into 100 mL of ethanol solution, and a certain amount of melamine was dispersed in 50 mL of ethanol at the same time. Secondly, the SiO_2-TiO_2 and melamine suspension were mixed and co-grounded using an ultrafine grinding mill. After grinding for 1 h, the SiO_2-TiO_2/melamine suspension was filtered and dried. Finally, the samples were calcined at 550 °C for 3 h to obtain SiO_2-TiO_2/CN composite. The as-prepared SiO_2-TiO_2/CN composite is marked as Si-Ti-CN-X, where X represents the mass ratio of melamine to SiO_2-TiO_2 (2.5, 3.75 and 5).

For comparison, the bulk CN was prepared through direct heating of melamine at 550 °C for 3 h, and the pure TiO_2 was prepared through the approach similar to the preparation of SiO_2-TiO_2 composite without SiO_2. The SiO_2/CN and TiO_2/CN samples were also prepared by the co-grinding of single SiO_2 or TiO_2 with melamine and the calcination of grinding product. Moreover, the SiO_2/P25/CN composite (Si-P25-CN-3.75) was also prepared by replacing SiO_2-TiO_2 with the mixture of SiO_2 and P25, according to the mentioned process. In addition, the physical mixture of SiO_2-TiO_2 and CN was obtained according to the proportion of each component in Si-Ti-CN-3.75, and it was recorded as Si-Ti-CN-3.75Mix. The detail information of the characterization methods, photocatalytic activity tests and photoelectrochemical measurement of the as-prepared samples is shown in Supporting information.

The morphologies of the as-prepared samples were characterized by SEM and TEM (Fig. 1). In Fig. 1a, the pure TiO_2 prepared without SiO_2 carrier exhibits serious aggregation morphology, which is in the size of about 5 μm. As can be observed from Fig. 1c, the single-particle size of most pure TiO_2 particles is in the range of dozens of nanometers. This indicates that the prepared TiO_2 is the aggregates formed by the agglomeration of its unit particles, which will undoubtedly decrease its specific surface area and the amounts of active sites. However, the TiO_2 particles prepared with SiO_2 as carrier exhibit monodisperse morphology (Fig. 1e), and the particle size is remarkably reduced to below 10 nm, indicating that SiO_2 has a significant effect on inhibiting the grain

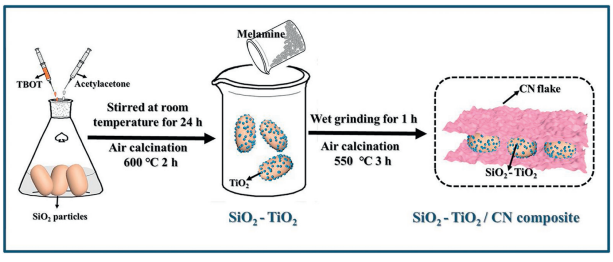

Scheme 1. Schematic illustration of synthesis strategy for SiO_2-TiO_2/CN composite photocatalyst.

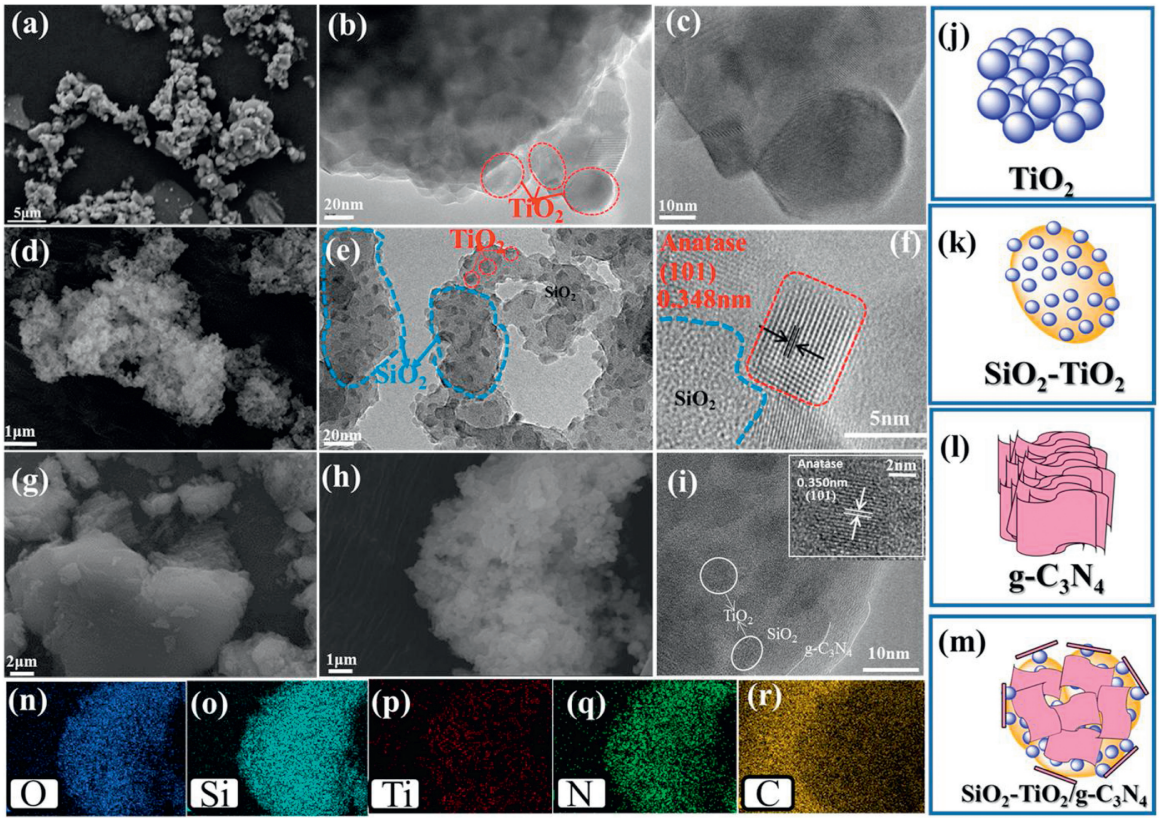

Fig. 1. (a) SEM, (b) TEM and (c) HRTEM images of pure TiO_2. (d) SEM, (e) TEM and (f) HRTEM images of SiO_2-TiO_2. (g) SEM image of bulk CN. (h) SEM and (i) HRTEM images of Si-Ti-CN-3.75. Morphology sketch image of (j) pure TiO_2, (k) SiO_2-TiO_2, (l) CN, (m) Si-Ti-CN-3.75 and the corresponding elemental mapping of (n) O, (o) Si, (p) Ti, (q) N and (r) C in (h).

growth and particle agglomeration of TiO_2. The above results may be attributed to the follows, SiO_2 has abundant surface hydroxyl groups, and the $TiO_2{\cdot}nH_2O$ (hydrolysates of TBOT) particles are more likely to combine with the surface hydroxyl groups of SiO_2 than to associate with themselves. This inhibits the growth of the TiO_2 and promotes the production of highly dispersed TiO_2 with small particle size during the calcination process. Fig. 1f shows the high-resolution TEM image of SiO_2-TiO_2 samples, where the lattice spacing of 0.348 nm matches the (101) plane of anatase, and the disorder area belongs to the amorphous structure of SiO_2. The semiconductor nanoparticles with smaller size always exhibit higher photocatalytic activity, due to the photo-generated carriers can transport to the surface more easily. Therefore, the monodisperse morphology of TiO_2 will certainly facilitate sufficient contact and the charge transmission between TiO_2 and CN. Fig. 1g exhibits the sheet-like morphology of CN, containing many stacking layers and is in size of several micrometers, indicating the agglomerate state of CN. However, in the SEM and TEM images of prepared Si-Ti-CN-3.75 (Figs. 1h and i), the bulk CN particles disappeared, and a great quantity of CN flakes with smaller lateral dimensions and thickness can be observed. The improvement of dispersivity and the morphology changes of CN in Si-Ti-CN-3.75 composite is attributed to the carrier effect of SiO_2. Besides, The HRTEM image in Fig. 1i shows the existence of the anatase TiO_2, and the lattice fringes of CN cannot be clearly seen due to its weak crystallinity. Compared with pure TiO_2, the crystallinity of the small TiO_2 loaded on the surface of SiO_2 is low, which will facilitate electronic migration between TiO_2 and CN because the similar crystal structure is one of the important factors to form efficient heterostructure. In Si-Ti-CN-3.75, the TiO_2 is at the scale of quantum dots (about 7 nm), and CN is presented with the lateral size of several hundred nanometers and the thickness below 100 nm. Therefore, the characteristics of the heterostructure formed by TiO_2 quantum dots and CN nanosheets are different from those formed by the bulk TiO_2 and CN. The morphology sketch images of pure TiO_2, SiO_2-TiO_2, CN and Si-Ti-CN-3.75 are shown in Figs. 1j–m. Obviously, the decreased size and the enhanced particle dispersion of TiO_2 and CN are caused by the introduction of SiO_2, which are the main factors for the performance enhancement of Si-Ti-CN composite photocatalysts.

The EDS mapping of corresponding elements in the Si-Ti-CN-3.75 composite is shown in Figs. 1n–r. It can be clearly observed that the Si, O, Ti, C and N elements are uniformly distributed in the Si-Ti-CN-3.75 region, confirming that the composite and heterostructure between SiO_2-TiO_2 and CN has successfully formed.

Fig. 2a shows the XRD patterns of SiO_2-TiO_2, CN and Si-Ti-CN-X composite photocatalysts. The characteristic peak of TiO_2 was observed at around 25.3° in all samples, which can be ascribed to the (101) plane of anatase TiO_2 [34]. The peak intensity of crystal-phase TiO_2 is relatively weak because the content of TiO_2 is low and the crystallinity of TiO_2 is poor due to its small particle size. In the XRD patterns of Si-Ti-CN-X, the peaks with 2θ values of 13.2° and 27.3° are corresponded to (100) and (002) planes of CN, indicating the existence of CN [35,36]. The intensity of these peaks increases with the increase of CN content. Additionally, a wide and weak peak in the range of 15°-25° can be observed in both SiO_2-TiO_2 and Si-Ti-CN-X samples, which are ascribed to the amorphous structure of SiO_2. The XRD results are consistent with those of HRTEM images, revealing that SiO_2-TiO_2 and CN have been successfully compounded. TGA analysis was carried out to investigate the content of CN in Si-Ti-CN-X samples, and the results are shown in Fig. 2b. It can be seen that there is an obvious weight-loss process between 500–700 °C in all samples, which is assigned to the decomposing of CN. The weight fraction of CN in

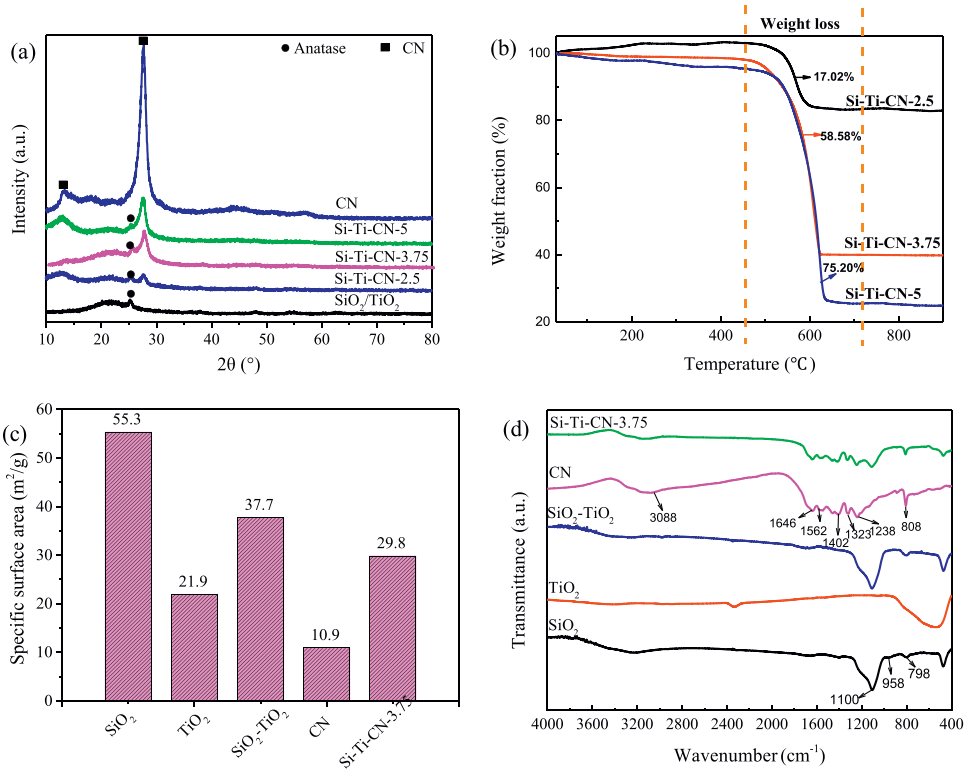

Fig. 2. (a) XRD patterns of SiO_2-TiO_2 and Si-Ti-CN-X. (b) TGA curves of Si-Ti-CN-X. (c) Specific surface areas and (d) FT-IR spectra of SiO_2, TiO_2, SiO_2-TiO_2, CN and Si-Ti-CN-3.75.

the composite was calculated through the weight loss fraction. It is 17.02%, 58.58% and 75.20% for Si-Ti-CN-2.5, Si-Ti-CN-3.75 and Si-Ti-CN-5, respectively.

As shown in Fig. 2c, the specific surface areas (A_{BET}) of SiO_2, TiO_2, SiO_2-TiO_2, CN and Si-Ti-CN-3.75 samples were investigated. Among the samples, SiO_2 has the highest surface area of 55.3 m^2/g. The high specific surface area and abundant surface hydroxyl groups endow SiO_2 with more active sites. It will facilitate the interfacial recombination of SiO_2 with other materials and the contact with the reactants in the photocatalytic process. Moreover, the A_{BET} of SiO_2-TiO_2 is 37.7 m^2/g, which is obviously higher than that of pure TiO_2. This is caused by the characteristics of SiO_2 and the improvement of the dispersivity of TiO_2 after compounding with SiO_2, which is consistent with TEM results. However, the A_{BET} of bulk CN is 10.9 m^2/g only, which is caused by the large scale and serious agglomeration of CN sheets. By comparison, the A_{BET} of Si-Ti-CN-3.75 is 29.8 m^2/g, which is around 3 times higher than that of CN. The result indicates that Si-Ti-CN-3.75 has obtained a high specific area through the supporting effect of SiO_2. This is beneficial to its photocatalytic performance improvement.

To investigate the combination properties between SiO_2, TiO_2 and CN, the FTIR spectra of raw materials and as-prepared composites were recorded (Fig. 2d). As for TiO_2, the strong adsorption below 850 cm^{-1} can be assigned to Ti—O—Ti bonds [37]. In the FT-IR spectrum of SiO_2, the peaks appearing at 1100 and 788 cm^{-1} are induced by the asymmetric and symmetric stretching of Si–O–Si bonds. The characteristic absorption peak of Si—OH presents at 958 cm^{-1} [38]. The broad absorption band in the range of 3100 cm^{-1} to 3600 cm^{-1} is ascribed to the O—H stretching. However, the characteristic absorption peak of Si—OH almost disappears in the spectrum of SiO_2-TiO_2. It is inferred that this may be induced by the dehydroxylation reaction occurred between the Si—OH and the surface hydroxyl groups absorbed in TiO_2. Several adsorption bands between 1200–1700 cm^{-1} can be clearly seen in the spectrum of CN, which are induced by the typical vibration of the C—N and C=C heterocycles [39]. The broad absorption band at 2800–3600 cm^{-1} is induced by the stretching vibration of N—H and surface adsorbed water. The adsorption peak originated from the particular breathing mode of triazine units presents at 808 cm^{-1}. The characteristic absorption peaks of SiO_2 and CN are both observed in the spectrum of Si-Ti-CN-3.75, indicating the compound of CN and SiO_2-TiO_2. Moreover, the absorption band of O—H in the spectrum of Si-Ti-CN-3.75 becomes wide and shows a slight redshift compared with that of CN. This may be caused by the reaction between N—H (or hydroxyl groups of adsorbed water) of CN and the hydroxyl groups of SiO_2 or TiO_2.

To further investigate the binding properties, the surface chemical composition and oxidation state of SiO_2-TiO_2, CN and Si-Ti-CN-3.75, the X-ray photoelectron spectroscopy of the samples was investigated, and the results are shown in Fig. 3. The Si, Ti, O, C and N elements are both observed in the survey spectrum of Si-Ti-CN-3.75 (Fig. 3a). The narrow scan C 1s spectrum of CN (Fig. 3b) can be fitted into three peaks at 285.01, 288.31 and 289.43 eV, which can be assigned to C atoms in C=C—C, N—C=N and C—O (induced by the surface absorbed water). The characteristic peaks of N atoms located at 400.10 and 398.57 eV can also be observed in the N 1s spectrum of CN (Fig. 3c) [40,41]. Compared with CN, there is no new peak appearing at the N 1s spectrum of Si-Ti-CN-3.75, indicating that the N atoms are not doped into the lattice of TiO_2. However, the binding energy of C and N elements in CN increases slightly after compounding with SiO_2-TiO_2, indicating the decrease of the density of the electron cloud. These results show that when TiO_2 and CN are in contact, the electrons tend to flow from CN to TiO_2. Thus, an internal electric field directed from CN to TiO_2 is formed. Therefore, the photo-electrons of TiO_2 can transfer to CN driven by the internal electric field under the light irradiation, which is consistent with the electron transfer path of the Z-scheme system.

In Figs. 3d and e, it can be seen that the binding energy of Si and O atoms in $SiO_2$is shifted after compounding with TiO_2 and CN,

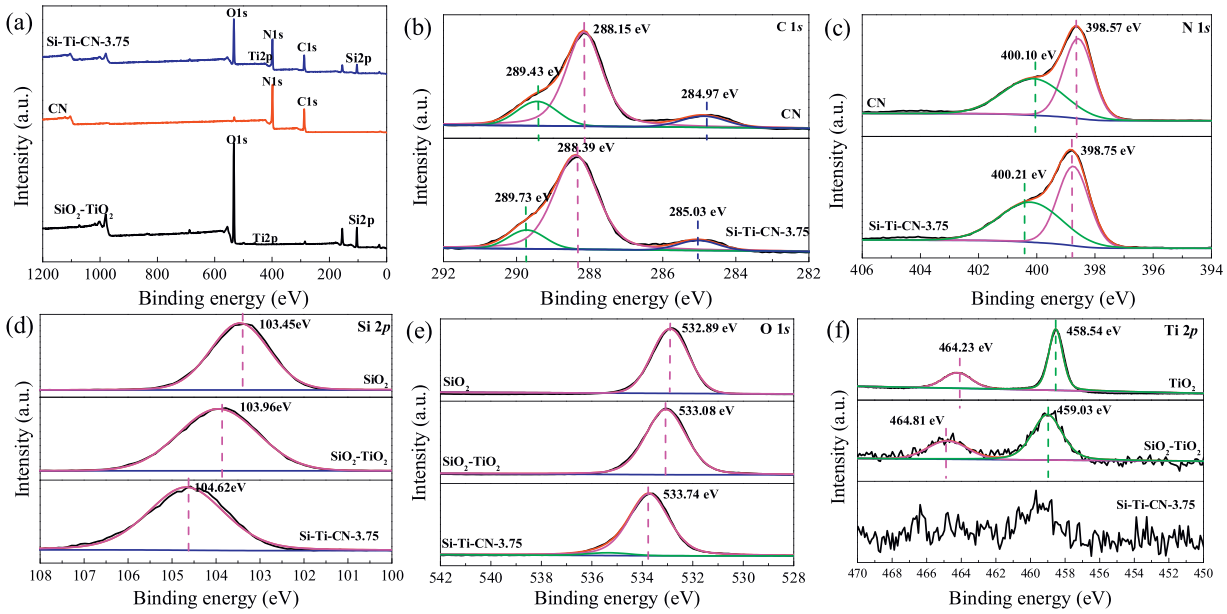

Fig. 3. (a) Wide scan XPS spectra of SiO_2-TiO_2, CN and Si-Ti-CN-3.75. Narrow scan XPS spectra of (b) C 1s, (c) N 1s for CN and Si-Ti-CN-3.75, (d) Si 2p, (e) O 1s for SiO_2, SiO_2-TiO_2 and Si-Ti-CN-3.75 and (f) Ti 2p for TiO_2, SiO_2-TiO_2 and Si-Ti-CN-3.75.

indicating the effective combination of SiO_2 with TiO_2 and CN. In the narrow scan spectrum of Ti 2p (Fig. 3f), an obvious displacement can be observed between the binding energy of Ti in TiO_2 and SiO_2-TiO_2. The reason may be that a large amount of Si-O-Ti bonds are formed at the interface of SiO_2 and TiO_2. Moreover, the characteristic peaks of Ti 2p in Si-Ti-CN-3.75 is much weaker than those in SiO_2-TiO_2, because the surface of Si-Ti-CN-3.75 is coated by g-C_3N_4 and the mass ratio of TiO_2 in Si-Ti-CN-3.75 is far less than that in SiO_2-TiO_2. Therefore, no obvious displacement can be observed between the binding energy of Ti 2p in SiO_2-TiO_2 and Si-Ti-CN-3.75 due to the disturbance of the wide peaks in Si-Ti-CN-3.75. As the electronegativity of Si atom is higher than that of Ti atom, it can induce the positively charged holes to move towards the Si-O-Ti interface and promote the directional separation of photogenerated electrons and holes. Therefore, the photo-electrons produced by TiO_2 can transfer to the interface between TiO_2 and CN, and then compound with the holes located at the valence band of CN. In the presence of SiO_2, the contact area of TiO_2 and CN increases, leading to a large number of electronic transmission channels formed between their interfaces, thus it can promote the formation of efficient Z-scheme heterostructure. According to the above analysis, the probable charge migration path in SiO_2-TiO_2/CN is established (Fig. S1 in Supporting information).

The optical property of the as-prepared Si-Ti-CN and contrastive samples was tested. Fig. S2a (Supporting information) shows the UV–vis diffuse reflectance spectra (DRS) results of TiO_2, SiO_2-TiO_2, CN and Si-Ti-CN-3.75. TiO_2 exhibits a strong light absorption at the UV region (below 400 nm) and it has nearly no light absorption at the visible light region, because of its wide bandgap of TiO_2 (3.2 eV). As for SiO_2-TiO_2, it exhibits a similar light absorption behavior to TiO_2, however, its absorption edge shows an obvious blue shift compared with TiO_2. It can be attributed to the quantum confinement of nano-TiO_2(below 10 nm) on the surface of SiO_2 [42]. The CN sample has strong absorption in both UV and visible region due to its relatively narrow bandgap (2.65 eV). The Si-Ti-CN-3.75 composite exhibits a stronger light absorption in both UV and visible region compared with CN. These results can be interpreted as follows: because of the supporting function of SiO_2, the particle size of CN is reduced and the dispersivity is improved, resulting in that more surfaces of CN are exposed to harvest more light. Meanwhile, the SiO_2 has a strong reflective effect on light, and it is inferred that the reflected light originates from SiO_2 could be absorbed by the photocatalyst on the surface of SiO_2 [43]. Obviously, the relatively stronger light absorption will promote more electron-hole pairs generated in the photocatalytic reaction, favoring the oxidation or reduction reaction. Furthermore, the bandgaps of these samples were estimated by Kubelka – Munk transformation, $\alpha h\upsilon = A(h\upsilon - Eg)^2$, where α represents the absorption coefficient, υ is the light frequency, Eg is the bandgap energy and A is a constant. The results are shown in Fig. S2b (Supporting information), it can be seen that the bandgaps of TiO_2 and CN are 2.65 and 3.20 eV respectively, being consistent with the literature [44].

In order to investigate the effect of SiO_2 on the heterostructure property between TiO_2 and CN, the photocurrent transient response and electrochemical impedance spectroscopy (EIS) were measured, and the results are shown as Figs. 4a and b respectively. It can reflect the charge separation efficiency and charge transfer resistance of SiO_2-TiO_2, CN, SiO_2/CN, TiO_2/CN and Si-Ti-CN-3.75. Fig. 4a shows that the Si-Ti-CN-3.75 sample exhibits the highest photocurrent transient intensity among all samples, while CN exhibits the lowest intensity. The photocurrent transient intensity of SiO_2/CN and TiO_2/CN is higher than that of CN but much weaker than that of Si-Ti-CN-3.75, which indicates that the coexistence of SiO_2 and TiO_2 is the key point for the superior properties of Si-Ti-CN-3.75. Meanwhile, as shown in Fig. 4b, the Si-Ti-CN-3.75 exhibits the smallest arc radiuses in comparison with that of other samples, indicating its smallest charge transfer resistance. It is inferred that the close contact between TiO_2 and CN lead to the high mobility of the photogenerated electron-hole pair [45]. Undoubtedly, the strong light response and small charge transfer resistance can lead to a better photocatalytic performance of Si-Ti-CN-3.75 than TiO_2/CN. This mainly results from the formation of efficient heterostructure between TiO_2 and CN based on the carrier effect of SiO_2.

The fluorescence spectrum was used to determine the electron-hole pair separation behavior of CN, SiO_2/CN, TiO_2/CN, Si-Ti-CN-3.75 and Si-Ti-CN-3.75Mix (Fig. 4c). Obviously, the bulk CN presents the highest PL intensity among all samples, indicating that CN has the lowest separation efficiency of electron-hole pairs. Compared with CN, the intensity of the emission peaks of TiO_2/CN

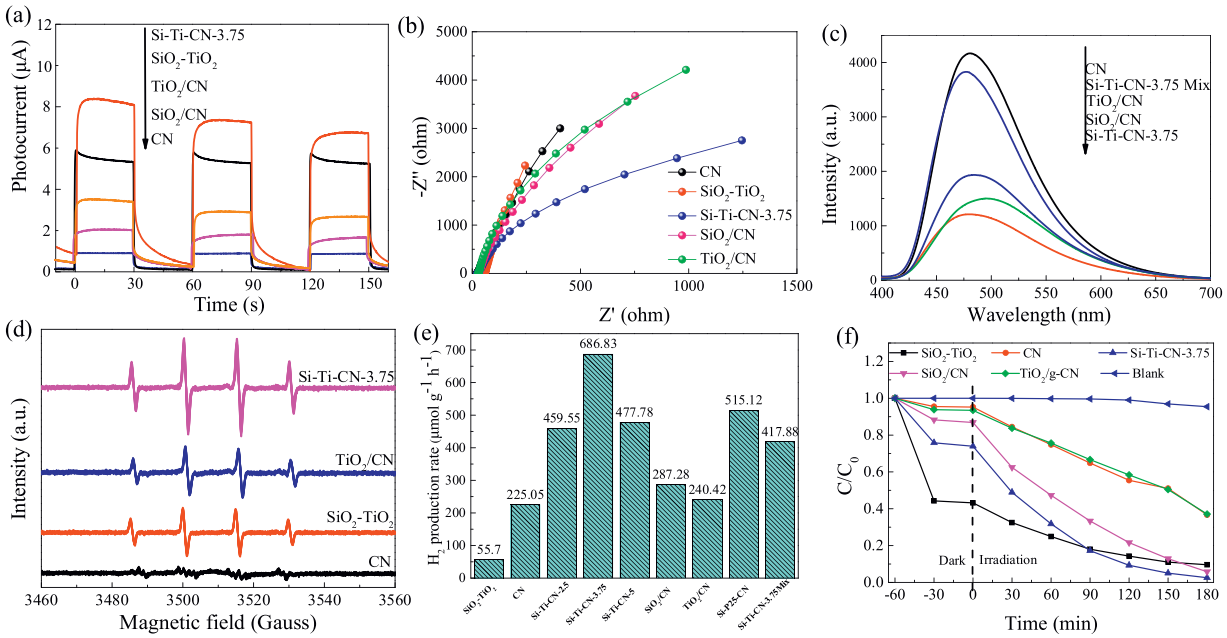

Fig. 4. (a) Transient photocurrent. (b) Nyquist plots of EIS. (c) PL spectra and (d) EPR spectra for the as-prepared composite as well as the comparative samples. (e) The photocatalytic H_2 production rate and (f) photocatalytic degradation of RhB of the as-prepared composite as well as the comparative samples under solar-like irradiation.

and SiO_2/CN have been significantly reduced. As for SiO_2/CN, it is mainly caused by that after compounding with SiO_2, the van der Waals forces between CN layers are weakened, which promotes more photogenerated carriers to migrate to the surface. Additionally, due to the negative electricity characteristic of the surface of SiO_2, SiO_2 also can capture some photogenerated carriers, thus inhibiting the recombination of electron-hole pairs [46]. It can be clearly seen that Si-Ti-CN-3.75 exhibits the lowest PL intensity among all samples, indicating the combination of SiO_2-TiO_2 and CN has improved the charge separation efficiency, and the improvement effect is stronger than that of TiO_2/CN composite. It indicates that a more efficient TiO_2-CN heterostructure has formed in SiO_2-TiO_2/CN than in TiO_2/CN.

To investigate the transition path of photo carriers in SiO_2-TiO_2/CN and TiO_2/CN, we measured the signal intensity of hydroxyl radicals ($^{\bullet}OH$) in SiO_2-TiO_2, CN, TiO_2/CN and Si-Ti-CN-3.75 under simulated solar light irradiation through EPR testing. In Fig. 4d, almost no signal can be observed in CN because it has the lower valance band potential (1.40 eV) than the potential of $OH^-/^{\bullet}OH$ (2.8 eV). Therefore, the holes in the valence band of CN cannot oxidize water or OH^- to $^{\bullet}OH$. For TiO_2, its valance band potential (2.90 eV) is slightly higher than that of $OH^-/^{\bullet}OH$ (2.8 eV). So it can oxidize water or OH^- to form $^{\bullet}OH$. Therefore, the signal of $^{\bullet}OH$ can be clearly observed in the EPR spectra ofSiO_2-TiO_2 [47]. In contrast to the SiO_2-TiO_2 and CN, the Si-Ti-CN-3.75 exhibits a much higher signal of $^{\bullet}OH$, indicating that more holes accumulate in the valance band of TiO_2 in Si-Ti-CN-3.75 because the holes at the valance band of CN cannot generate $^{\bullet}OH$. The increase of the holes at the valance band of TiO_2 is caused by the recombination between the electrons in the conduction band of TiO_2 and the holes in the valence band of CN, which can improve the separation efficiency of photogenerated electrons and holes. These results indicate that a Z-scheme heterostructure rather than a type II heterostructure has formed between TiO_2 and CN in SiO_2-TiO_2/CN, and several related literatures have confirmed the formation of Z-scheme heterostructure based on the similar discussion [48–50]. In contrast, the signal intensity of $^{\bullet}OH$ in TiO_2/CN is slightly lower than that of SiO_2-TiO_2.This indicates that the direct combination of TiO_2 and CN has no significant effect on the formation of $^{\bullet}OH$, confirming that there is no efficient Z-scheme heterostructure formed. It can be concluded that the presence of SiO_2 plays an important role in the formation of efficient Z-scheme heterostructure between TiO_2 and CN. In general, the Z-scheme heterostructure has a better photocatalytic redox performance than the traditional type II heterostructure because the photoelectrons and holes are located at the conduction of CN and the valance band of TiO_2 respectively, and they have a more negative reduction potential (−1.12 eV) and more positive oxidation potential (2.90 eV).

In order to further verify the effect of SiO_2 on promoting the interaction between TiO_2 and CN and improving the quality of the TiO_2/CN heterostructure, the photocatalytic H_2 production and RhB degradation performance of the samples are evaluated. As shown in Fig. 4e, the SiO_2-TiO_2 exhibits a negligible H_2 production performance with the H_2 production rate of 55.7 μmol g^{-1} h^{-1}, owing to the low content of TiO_2 and the narrow light harvest range. While CN shows an H_2 production rate of 225.05 μmol g^{-1} h^{-1}. In contrast, the H_2 production rate is significantly enhanced for the Si-Ti-CN-X composites, and the Si-Ti-CN-3.75 exhibits the highest H_2 production rate, which is 12.3 and 3.1times higher than SiO_2-TiO_2 and CN respectively (the photocatalytic active component in Si-Ti-CN-3.75 is only about 60 wt%). The H_2 production rate of Si-Ti-CN-3.75 is 686.83 μmol g^{-1} h^{-1}, which also can be calculated as about 1144.72 μmol g^{-1} h^{-1} for TiO_2/CN because the SiO_2 does not have the H_2 production ability. The H_2 production rate of TiO_2/CN in Si-Ti-CN-3.75 is higher than that of the Z-scheme photocatalyst reported by the related literature under solar-like irradiation, such as 625.5 μmol g^{-1} h^{-1} for C-doped g-C_3N_4@C, N co-doped TiO_2 core-shell heterojunction photocatalyst [51], 301.25 μmol g^{-1} h^{-1} for ZnO/ZnS/g-C_3N_4 nanocomposite [52], and 186.3 μmol g^{-1} h^{-1} for $ZnIn_2S_4$-Au-TiO_2photocatalysts [53]. This is mainly ascribed to that an efficient heterostructure has formed between SiO_2-TiO_2 and CN, which will accelerate the separation and transfer of photogenerated charge carriers. Besides, SiO_2/CN shows a slightly better hydrogen evolution performance than that of CN, confirming that the introduction of SiO_2 has a positive effect on the photocatalytic activity of CN, which could be attributed to the improvement of specific surface area and optical absorption performance of CN by SiO_2. More importantly, the TiO_2/

CN exhibits a much lower H_2 production performance compared with that of Si-Ti-CN-3.75. This result indicates the important effect of SiO_2 on the performance improvement of TiO_2/CN heterostructure. Moreover, the H_2 production rate of Si-Ti-CN-3.75 is also higher than that of Si-P25-CN-3.75, showing that the composite compounded from SiO_2-TiO_2 and CN has a better photocatalytic performance than the composite compounded from SiO_2, P25 and CN. This result confirmed the importance of the monodisperse TiO_2 loaded on the surface of SiO_2 and the close interface combination of SiO_2 and TiO_2 in Si-Ti-CN-3.75. The cyclic experimental results of Si-Ti-CN-3.75 for photocatalytic hydrogen production are shown in Fig. S3 (Supporting information). It is found that the hydrogen production rate of Si-Ti-CN-3.75 remains almost no change after three cycles, indicating its high stability.

The photocatalytic performance of the as-prepared samples was also evaluated by the degradation effect of RhB under solar-like irradiation (Fig. 4f). Similar to the results of photocatalytic H_2 production, the Si-Ti-CN-3.75 composite exhibits the best degradation performance for RhB among all the contrastive samples, and 98% of RhB was removed after 180 min irradiation in its presence. Besides, Si-Ti-CN-3.75 sample also shows strong adsorption property in the dark reaction. It may result from the ample adsorption and reaction sites on the surface of SiO_2, which is consistent with the specific surface area result. As indicated in Fig. S4 (Supporting information), the photocatalytic degradation follows the first-order kinetics. The slope of the lines in Fig. S4 represents the reaction rate constant (min^{-1}). It can be seen that the reaction rate constant of Si-Ti-CN-3.75 is 0.0189 min^{-1}, which is 3.9 times higher than TiO_2/CN, indicating the synergism of SiO_2, TiO_2 and CN ternary structure for Si-Ti-CN performance enhancement. The reaction rate constant of Si-Ti-CN-3.75 (0.0189 min^{-1}) is also higher than that of several g-C_3N_4 based photocatalyst reported by literature, such as 0.0100 min^{-1} for $(BiO)_2CO_3$/g-C_3N_4 [54], 0.01330 min^{-1} for g-C_3N_4/TiO_2/diatomite [55], and 0.0045 min^{-1} for g-C_3N_4 nanosheets/TiO_2 nanotube arrays [56]. This result confirms that Si-Ti-CN-3.75 is an ideal photocatalyst for organic pollutant degradation. As confirmed by both photocatalytic H_2 production and RhB degradation results, SiO_2 has dual functions on the performance improvement of Si-Ti-CN-3.75. On the one hand, it can improve the performance of the Si-Ti-CN-3.75 directly through improving its surface are and light adsorption. On the other hand, it can significantly improve the photocatalytic activity by promoting the close combination of TiO_2 and CN to construct efficient heterostructure indirectly

Based on the above analysis, the photocatalytic mechanism of SiO_2-TiO_2/CN composite was proposed. As shown in Scheme 2, with the presence of SiO_2 carrier, an efficient Z-scheme heterostructure formed between TiO_2 and CN through their close interfacial combination. Under the solar-like irradiation, electrons in the valence band of TiO_2 and CN are excited and transferred to their conduction band respectively, and the holes are left in the valence band. The excited electrons of TiO_2 recombine with the holes of CN. It weakens the tendency of the recombination of the electron-holes of CN and promotes more electrons remaining in the conduction band of CN. Meanwhile, the holes accumulated in the valence band of TiO_2 to take part in the oxidation reaction. The formation of Z-scheme heterostructure can significantly improve the separation and transport efficiency of photogenerated carriers. It is one of the important factors leading to the improved photocatalytic redox performance of SiO_2-TiO_2/CN than CNand-TiO_2/CN. The amorphous SiO_2 in SiO_2-TiO_2/CN has abundant surface hydroxyl groups and high surface activity, playing an important role in improving the photocatalytic performance. Firstly, the existence of SiO_2 promotes the formation of monodisperse TiO_2 nanoparticles with the particle size below 10 nm. Therefore, more surfaces of TiO_2 are exposed to contact and combination with CN. The large contact area between TiO_2 and CN endows more photocarrier transfer passways at their interface, great favoring the efficient photocarrier migration between TiO_2 and CN under the internal electric field. Moreover, the crystallinity of the TiO_2 is weakened by the reduction of particle size, which reduces the structural difference between TiO_2 and weakly crystallized CN, thereby can improve the efficiency of the heterostructure. Secondly, the better combination between SiO_2 and TiO_2 promotes the formation of large amount of Si–O–Ti interfaces. This has a positive effect on inducing the directional separation of photogenerated electron holes. Thirdly, SiO_2 has a strong reflective effect on light, which can increase the light absorption of the composite and facilitate the photocatalytic reaction.

In summary, SiO_2-TiO_2/CN composite photocatalyst was prepared through the sol-gel method associated with the wet-grinding process. Under solar-like irradiation, the SiO_2-TiO_2/CN (58.58 wt% of CN) composite shows several times higher photocatalytic hydrogen production and RhB degradation rate than TiO_2/CN and CN. The improved photocatalytic performance of SiO_2-TiO_2/CN can be attributed to the synergistic effect of the carrier effect of SiO_2 and the formation of efficient TiO_2/CN Z-scheme heterostructure. In SiO_2-TiO_2/CN, the existence of SiO_2 can increase the specific surface area and light absorption of SiO_2-TiO_2/CN, thus further improve the photocatalytic efficiency. More importantly, the particle size of TiO_2 and CN can be significantly reduced based on the carrier effect of SiO_2, which will increase the contact area and structural matching degree between TiO_2 and CN. Therefore, the quality and efficiency of TiO_2/CN heterostructure can be improved. Based on this study, the SiO_2 can serve as an effective carrier with multiple functions on the performance improvement of semiconductor photocatalyst. We believe that the SiO_2 can also be introduced into other semiconductor heterostructure systems to form a series of efficient ternary composite photocatalyst, which will be beneficial to developing highly efficient and low-cost photocatalysts.

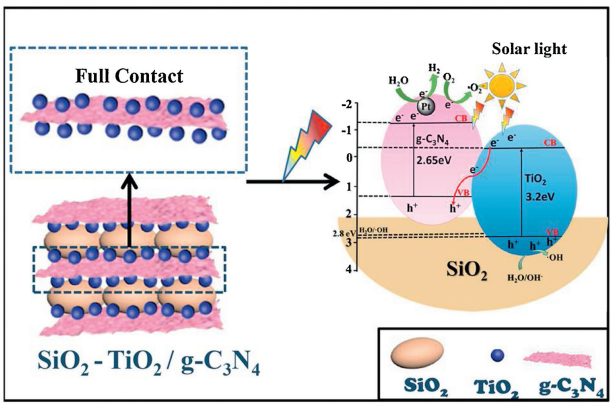

Scheme 2. Schematic diagram of the enhancement mechanism for photocatalysis performance of SiO_2-TiO_2/CN composite under solar-like irradiation.

Declaration of competing interest

The authors declare that they have no known competing financial interests or personal relationships that could have appeared to influence the work reported in this paper.

Acknowledgment

This work was partly supported by the National Natural Science Foundation of China (Nos. 21577132, 21978276).

Appendix A. Supplementary data

Supplementary material related to this article can be found, in the online version, at doi:https://doi.org/10.1016/j.cclet.2020.03.026.

References

[1] J.A. Turner, Science 305 (2004) 972–974.
[2] C.C. Dong, J.H. Ji, Z. Yang, et al., Chin. Chem. Lett. 30 (2019) 853–862.
[3] L. Mao, X.Y. Cai, S.Q. Yang, K. Han, J.Y. Zhang, Appl. Catal. B: Environ. 242 (2019) 441–448.
[4] W. Yan, Y. Yu, H.H. Zou, et al., Sol. RRL 2 (2018) 1800058.
[5] M. Xiao, B. Luo, S.C. Wang, L.Z. Wang, J. Energy Chem. 27 (2018) 1111–1123.
[6] M.X. Ran, P. Chen, J.R. Li, et al., Chin. Chem. Lett. 30 (2019) 875–880.
[7] R.R. Wang, X. Zhang, F. Li, et al., J. Energy Chem. 27 (2018) 343–350.
[8] Q. Hao, S.M. Hao, X.X. Niu, et al., Chin. J. Catal. 38 (2017) 278–286.
[9] Q. Hao, C.A. Xie, Y.M. Huang, et al., Chin. J. Catal. 41 (2020) 249–258.
[10] C.Q. Li, Z.M. Sun, W.Z. Zhang, C.H. Yu, S.L. Zheng, Appl. Catal. B: Environ. 220 (2018) 272–282.
[11] J. Wang, Y. Xia, H.Y. Zhao, et al., Appl. Catal. B: Environ. 206 (2017) 406–416.
[12] J.Y. Zhang, Y.H. Wang, J. Jin, et al., ACS Appl. Mater. Interfaces 5 (2013) 10317–10324.
[13] X.H. Li, J.S. Chen, X.C. Wang, J.H. Sun, M. Antonietti, J. Am. Chem. Soc. 133 (2011) 8074–8077.
[14] P. Zhou, J.G. Yu, M. Jaroniec, Adv. Mater 26 (2014) 4920–4935.
[15] W.L. Yu, D.F. Xu, T.Y. Peng, J. Mater. Chem. 3 (2015) 19936–19947.
[16] T.M. Di, B.C. Zhu, B. Cheng, J.G. Yu, J.S. Xu, J. Catal. 352 (2017) 532–541.
[17] W.L. Yu, J.X. Chen, T.T. Shang, et al., Appl. Catal. B: Environ. 219 (2017) 693–704.
[18] P. Zhang, M. Fujitsuka, T. Majima, J. Energy Chem. 25 (2016) 917–926.
[19] L.N. Ma, G.H. Wang, C.J. Jiang, H.L. Bao, Q.C. Xu, Appl. Surf. Sci. 430 (2018) 263–272.
[20] H. Wang, Y.H. Liang, L. Liu, J.S. Hu, W.Q. Cui, J. Hazard. Mater. 344 (2018) 369–380.
[21] W. Zhen, F.F. Liang, Y.F. Liu, et al., Appl. Catal. B: Environ. 201 (2017) 600–606.
[22] Q.H. Liang, Z. Li, Y. Bai, et al., Small 13 (2016) 1603182.
[23] F.J. Wu, X. Lin, W. Liu, S.T. Zhang, Appl. Surf. Sci. 405 (2017) 60–70.
[24] Y.J. Zou, J.W. Shi, D.D. Ma, et al., ChemCatChem 9 (2017) 3752–3761.
[25] Z.A. Huang, Q. Sun, K.L. Lv, et al., Appl. Catal. B: Environ. 164 (2015) 420–427.
[26] W. Jo, T.S. Natarajan, Chem. Eng. J. 281 (2015) 549–565.
[27] W. Zhao, L.L. Feng, R. Yang, J. Zheng, X.G. Li, Appl. Catal. B: Environ. 103 (2011) 181–189.
[28] X.X. Wang, S.S. Wang, W.D. Hu, et al., Mater. Lett. 115 (2014) 53–56.
[29] Y. Zhang, J.R. Chen, H. Tang, et al., J. Hazard. Mater. 354 (2018) 17–26.
[30] L. Pinho, M.J. Mosquera, Appl. Catal. B: Environ. 134-135 (2013) 205–221.
[31] B. Lin, C. Xue, X.Q. Yan, G. Yang, B.L. Yang, Appl. Surf. Sci. 357 (2015) 346–355.
[32] P. Wilhelm, D. Stephan, J. Photochem. Photobiol. A: Chem. 185 (2007) 19–25.
[33] Y. Chen, H. Ding, S.J. Sun, Nanomaterials 7 (2017) 217.
[34] K. Klaus, T. Tuomas, J. Hazard. Mater. 155 (2009) 466–473.
[35] H.J. Yu, R. Shi, Y.X. Zhao, et al., Adv. Mater. 29 (2017) 1605148.
[36] Q.H. Liang, Z. Li, Z.H. Huang, F.Y. Kang, Q.H. Yang, Adv. Funct. Mater. 25 (2015) 6885–6892.
[37] M.Q. Hu, Y. Cao, Z.Z. Li, S.L. Yang, Z.P. Xing, Appl. Surf. Sci. 426 (2017) 734–744.
[38] S. Bruni, F. Cariati, M. Casu, et al., Nanostruc. Mater. 11 (1999) 573–586.
[39] G. Miao, D.S. Huang, X.L. Ren, et al., Appl. Catal. B: Environ. 192 (2016) 72–79.
[40] S.X. Yu, J.Y. Li, Y.H. Zhang, et al., Nano Energy 50 (2018) 383–392.
[41] X. Yu, X.L. Fan, L. An, et al., Carbon 128 (2018) 21–30.
[42] D.L. Pan, Z.Y. Han, Y.C. Miao, D.Q. Zhang, G.S. Li, Appl. Catal. B: Environ 229 (2018) 130–138.
[43] C.Q. Li, Z.M. Sun, X. Li, L.X. Liu, S.L. Zheng, Adv. Powder Technol. 27 (2016) 2051–2060.
[44] T. Giannakopoulou, I. Papailias, N. Todorova, et al., Chem. Eng. J. 310 (2017) 571–580.
[45] Z.F. Xu, K. Xu, H.F. Feng, Y. Du, W.C. Hao, Sci. Bull. 63 (2018) 465–468.
[46] Q. Hao, X.X. Niu, C.S. Nie, et al., Phys. Chem. Chem. Phys. 18 (2016) 31410–31418.
[47] J. Li, M. Zhang, Q.Y. Li, J.J. Yang, Appl. Surf. Sci. 391 (2017) 184–193.
[48] W.K. Jo, T.S. Natarajan, Chem. Eng. J. 281 (2015) 549–565.
[49] Y.H. Li, K.L. Lv, W.K. Ho, et al., Appl. Catal. B: Environ. 202 (2017) 611–619.
[50] K. Hu, R.Q. Li, C.N. Ye, et al., J. Clean. Prod. 253 (2020) 120055.
[51] M.A. Mhamed, M.F. Zain, L.J. Minggu, et al., Appl. Surf. Sci. 476 (2019) 205–220.
[52] Z.F. Dong, Y. Wu, N. Thirugnanam, G.L. Li, Appl. Surf. Sci. 430 (2018) 293–300.
[53] G. Yang, H. Ding, D.M. Chen, et al., Appl. Catal. B: Environ. 234 (2018) 260–267.
[54] J. Huang, H.H. Liu, J.F. Chen, et al., Mat. Sci. Semicon. Proc. 82 (2018) 97–103.
[55] Z.M. Sun, C.Q. Li, G.Y. Yao, S.L. Zheng, Mater. Design 94 (2016) 403–409.
[56] D.T. Zhou, Z. Chen, Q. Yang, ChemCatChem 8 (2016) 3064–3073.